Heliyon 7 (2021) e08494

Contents lists available at ScienceDirect

Heliyon

journal homepage: www.cell.com/heliyon

Research article

Hydrogen storage in purified multi-walled carbon nanotubes: gas hydrogenation cycles effect on the adsorption kinetics and their performance

Edgar Mosquera-Vargas [a,b,*], Rocío Tamayo [c], Mauricio Morel [d], Martín Roble [e], Donovan E. Díaz-Droguett [e,f,g,**]

[a] Grupo de Transiciones de Fase y Materiales Funcionales, Departamento de Física, Universidad del Valle, Santiago de Cali, Colombia
[b] Centro de Excelencia en Nuevos Materiales (CENM), Universidad del Valle, A.A. 25360, Santiago de Cali, Colombia
[c] Escuela Profesional de Ingeniería de Materiales, Facultad de Ingeniería de Procesos, Universidad Nacional de San Agustín, Av. Venezuela S/N, Arequipa, Peru
[d] Facultad de Ciencias Naturales and Instituto de Investigaciones Científicas y Tecnológicas (IDICTEC), Universidad de Atacama, Av. Copayapu 485, Copiapó, Chile
[e] Instituto de Física, Facultad de Física, Pontificia Universidad Católica de Chile, Casilla, 306, Santiago, Chile
[f] Centro de Investigación en Nanotecnología y Materiales Avanzados, CIEN UC, Pontificia Universidad Católica de Chile, Santiago, Chile
[g] Centro de Energía UC, Pontificia Universidad Católica de Chile, Santiago, Chile

ARTICLE INFO

Keywords:
Purified carbon nanotubes
Specific surface area (SSA)
Raman spectroscopy
Hydrogen storage

ABSTRACT

Multi-walled carbon nanotubes (MWCNTs) are an alternative for storage with low cost, eco-friendly, and good performance for both process adsorption and desorption. Herein, a purification procedure of MWCNTs was successfully described and studied by using XRD, TEM, Raman spectroscopy and by means of N_2 adsorption-desorption isotherms using the BET method. The H_2 storage properties at room temperature of the purified carbon nanotubes exposed to gas under pressures between 0.39 and 13.33 kPa was investigated by using the quartz crystal microbalance technique. It was found that the H_2 adsorption capacity is strongly dependent on the morphological and structural characteristics of the carbon nanotubes and their specific surface area. The best sample with specific surface area of $729.4 \pm 3\ m^2\ g^{-1}$ shows a maximum adsorption capacity of 3.46 wt% at 12.79 kPa of H_2 exposure pressure. The adsorption kinetics ($t_{95\%}$) from the different purified MWCNTs was also investigated as a function of the H_2 exposure pressure as well as the performance of these MWCNTs on the reversibility of the H_2 loading/unloading process when underwent to successive cycles of gas exposure.

1. Introduction

Clean and sustainable energy is one of the principal foci of the economic development of national economies, whose principal aim meets the need of increasing energy supplies due both to the growth of the world population and to environmental issues [1, 2, 3, 4]. Therefore, hydrogen as an ecofriendly energy vector can be an efficient alternative to fulfill the energy demands. However, the three forms hydrogen storage: compressive gas, cryogenic liquid, and solid-state storage, are a major challenge for storage and transportation [5]. Hydrogen production from solar energy is a target to obtain clean energy from renewable energies. The coming paradigm change must be accompanied by the development of new materials to incorporate hydrogen in the energetic matrix of society. Production and storage of this energy can involve novel rechargeable batteries and the development of devices for H_2 storage and compression of H_2 gas. In this way, some of the promising materials identified are metal hydrides, chemical H_2 storage and sorbent materials (MOF and carbon nanotubes) [3, 6, 7]. To this end several investigations [5, 8] focus on research of hydrogen storage in solid-state form, due economical and safety considerations, where hydrogen combines with materials and alloys through physisorption or chemisorption.

Over the last years, there has been a research interest of the scientific community in the synthesis of carbon nanotubes (CNTs) due to its wide spectrum of application [4, 5, 7, 8, 9, 10] as well on the hydrogen storage problem. Since the discovery of carbon nanotubes (CNT) by Iijima [11], carbonaceous materials and mainly CNTs are the most widely used materials for the study and storage of hydrogen [3, 7, 8, 9, 10, 12, 13, 14, 15, 16, 17]. But, although their adsorption properties have been studied

* Corresponding author.
** Corresponding author.
E-mail addresses: edgar.mosquera@correounivalle.edu.co (E. Mosquera-Vargas), dodiaz@fis.puc.cl (D.E. Díaz-Droguett).

https://doi.org/10.1016/j.heliyon.2021.e08494
Received 6 June 2021; Received in revised form 15 September 2021; Accepted 24 November 2021

experimentally, the mechanism of the hydrogen storage capacity of CNTs is not yet clear [3, 12, 16, 17]. Thus, several research groups have carried out theoretical and experimental studies achieving remarkable progress to reach the benchmark of 5.5 wt% with a volumetric capacity of 40 g of H_2/L, set by the US Department of Energy (DoE) for the year 2025 and ultimate full fleet (UFF) of 50 g of H_2/L for hydrogen storage on-board automobile application [3, 18]. However, an effort has been made by the scientific community to solve this problem in order to find a solution. The situation that the DoE benchmark has not been achieved makes this issue an interesting and very relevant topic for research.

Research on H_2 storage in carbon materials, such as graphene and graphene oxide (GO), single walled- and multi walled-carbon nanotubes (SWCNTs, MWCNTs, and purified), carbon nanofibers (CNFs), and activated carbon (AC) has been dominated by announcements of high storage capacities in carbon nanostructures [3, 17, 19]. The storage of hydrogen in solid materials such as carbonaceous materials (GO, SWCNTs, MWCNTs, CNFs, and AC), can be carried out through physisorption or chemisorption, which present high H_2 storage capacity due to their high specific surface area (SSA) and low mass density [3, 19, 20]. Thus, the capacity of physisorption-based hydrogen storage in carbon materials depends on its pore size (micropores (<2 nm), mesopores (2–50 nm) and macropores (>50 nm)). Therefore, theoretical and experimental studies on hydrogen storage of carbonaceous materials and carbon-based hybrid structures are continually being studied [3, 12, 15, 16, 17, 21, 22]. Recent studies reported that the H_2 storage capacity for carbon materials is less than 10 wt% [3, 12, 15, 16, 17, 23, 24, 25, 26, 27, 28, 29, 30, 31, 32, 33, 34], the values obtained so far have not reached the required DoE benchmark. Furthermore, the great challenge of finding a material capable of storing enough hydrogen under ambient conditions remains.

Nevertheless, it is believed that the growth method and synthesis conditions [34], purification [35, 36, 37, 38], and structure (with high specific surface area (SSA) and large free pores volume) [3, 17, 19] of carbon-based architectures, such as CNTs, could have a strong effect on hydrogen storage capacity and adsorption kinetics. Due to synthesis methods, the fabricated CNTs present impurities such as metal catalyst and carbonaceous materials in the final product, consequently it is important to reduce or eliminate these impurities in the as-grown CNTs, depending on the application field. The purification has an important effect on adsorption process in carbon nanotubes [37, 38] and several methods have been reported and modified to remove these impurities. However, different purification methods have been used to modify CNTs and to improve their hydrogen storage capacity and adsorption behavior [35, 36, 37, 38]. Moreover, the type of CNTs, the types and defects density, the number of walls, and pores sizes are important parameters to clarify.

In this work, multi-walled carbon nanotubes grown by aerosol assisted chemical vapor deposition (AACVD) and purified have been characterized by different techniques to study their structure, specific surface area (SSA), grade of graphitization and quality of them, respectively. The hydrogen storage capacity and adsorption kinetics were studied by using a quartz crystal microbalance (QCM) technique. The maximum adsorption capacity achieved at room temperature was 3.46 wt. % at 12.79 kPa of H_2 exposure pressure. The results indicate that MWCNTs synthesized and purified in this research present excellent adsorption performance, considering that they were studied under a range of low hydrogen exposure pressures. In future work, studies on the hydrogen storage capability and adsorption kinetics under higher H_2 exposure pressures will be carried out for comparative analysis.

2. Experimental details

2.1. Carbon nanotubes growth

Multi-walled carbon nanotubes (MWCNTs) were grown by using aerosol-assisted CVD (AACVD) method. The experimental synthesis parameters (catalyst/support proportion and carrier gas) used are reported in Table 1 and Ref. [15, 16]. When the system was cooled naturally to room temperature (RT), the blackened powder was collected for characterization without purification process (see Ref [15, 16]).

2.2. Carbon nanotubes purification process

The purification process of the samples was carried out using fluorhydric acid (HF) and chlorhydric acid (HCl) to determine the effect of the purification of the MWCNTs on the impurity phases present and hydrogen storage properties. Figure 1 shows the schematic diagram of the purification process. First (Step:1), a quantity of MWCNTs (~500 mg) was placed in a tubular furnace at 450 °C for 1 h (rate: 15 °C/min) and after that, the system was cooled down to room temperature (RT) by its own thermal inertia. XRD was employed to characterize the samples. Subsequently, the MWCNT samples are immersed in an HF solution at a volume ratio (HF: MWCNT) of 1: 3 and sonicated for 1 h (Step 2). Afterwards, deionized water was used to clean the MWCNTs with centrifugation at 3500 rpm to obtain a pH neutral value of the solution (Step 3). The samples were then dried (Step 4) in an oven for 48 h at room temperature to characterize them by XRD. In Step 5, the MWCNT samples are immersed in a HCl solution at a volume ratio (HCl:MWCNTs) of 1:3 for 24 h at RT. In Step 6 the samples were thoroughly washed with deionized water and centrifuged to obtain a pH neutral value. Finally (Step 7), the MWCNT samples were dried in a vacuum oven at 80 °C for 1 h.

2.3. Characterization techniques

The phase purity and the crystallinity of the prepared samples were characterized at room temperature (RT) using a Bruker D8 X-ray diffractometer with CuKα radiation. The X-ray diffractometer was operated at 45 kV and 40 mA, with 2θ within the range of 2°–80° and step size of 0.01°. Thermogravimetric analysis (TGA) of carbon nanotubes (MWCNTs) was carried out with a TA Instruments, TGA Q50, under nitrogen (N_2) gas and heated from room temperature (RT) to 800 °C with a rate of 10 °C min^{-1}. The specific surface area (SSA) and the pore dimension of the carbon nanotubes were determined by N_2 adsorption-desorption isotherms at –196 °C in a Micromeritics ASAP 2010. Raman scattering were recorded at RT using a LabRam 010 from ISA to identify the structure and crystallinity of purified carbon nanotubes. A He–Ne laser at 632.8 nm with a nominal power of 5.5 mW was used as the Raman excitation source.

Structural characterization was done by high-resolution transmission electron microscope (HRTEM, Tecnai F20 FEG-S/TEM) operated at 200 kV. TEM samples were ultrasonically dispersed in isopropyl alcohol and then collected in an ultrathin holey carbon-coated Cu grid.

2.4. Hydrogen adsorption microgravimetric measurements

The H_2 adsorption capability studies of the highly purified MWCNTs were performed by means of a microgravimetric technique using a quartz crystal microbalance (from MDC model SQM-310) placed inside a vacuum chamber adapted with gas injection lines and pressure gauges (Figure 2), as described in our previous work on hydrogen adsorption studies [15, 16]. For this technique a quartz crystal microbalance (QCM)

Table 1. The experimental condition and X-ray structural parameters after of thermal treatment in purified MWCNTs.

Sample	Catalyst	Support	Carrier gas	2θ (°)	Layer distance (nm)
CNT11	Ni	—	N_2	26.05	0.3416
CNT12	Ni	Zeolite	N_2	26.16	0.3424
CNT13	Ni	Zeolite	Ar	26.13	0.3406
CNT14	Magnetite (80%)	—	Ar	26.02	0.3420
CNT15	Magnetite (90%)	Zeolite	Ar	25.85	0.3443

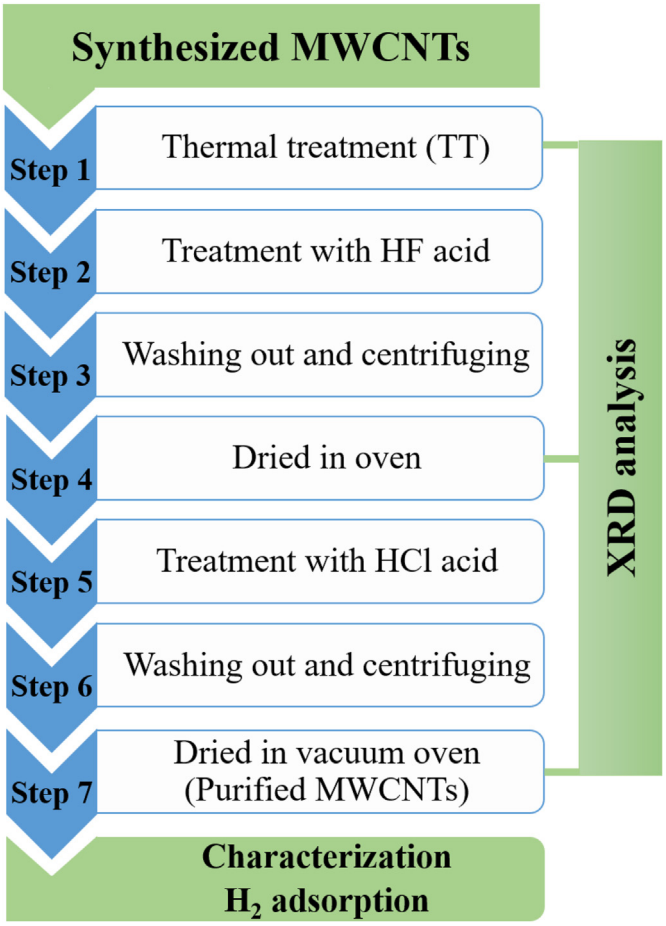

Figure 1. Schematic diagram of the purification process.

Table 2. Weight loss after of thermal treatment in purified MWCNTs.

Sample	Initial Mass	Final Mass	Δm	Weight loss %
CNT11	0.558	0.554	0.004	0.72
CNT12	0.632	0.582	0.050	7.91
CNT13	0.569	0.565	0.004	0.70
CNT14	0.527	0.526	0.001	0.19
CNT15	0.400	0.395	0.005	1.25

was used as supporting substrate where the purified MWCNTs is deposited. The experimental procedure here is the following: first, the purified MWCNTs powder is dispersed in isopropyl alcohol by sonication using an ultrasonic bath for about 5 min. Next, the suspension is deposited onto the QC top-face and dried under air at RT. The sample-loaded QC was placed in the working head of the microbalance system and transferred into the vacuum chamber. Then, the chamber was pumped down to $\sim 1.19 \times 10^{-7}$ kPa using turbo and rotatory pumps working in series. For the gas adsorption measurements, a gate valve placed between the chamber and the turbo pump was used to isolate the chamber, this allowed pressurization with H_2 gas (Indura, 99.995 %, $O_2 < 5$ ppm, $H_2O < 8$ ppm, $CO_2 + CO < 4$ ppm, $N_2 < 20$ ppm and THC <5 ppm); the gas flow was controlled through a manual needle valve. When exposed to H_2 the sample adsorb a certain amount of the gas, which translates into a gain of mass by the loaded-QC. These changes in mass are monitored in real-time by recording the resonance frequency of the QC. The purified MWCNTs samples were exposed to hydrogen for 8 min under a working pressure from 0.39 up to 13.33 kPa, measured with a capacitive gauge (Baratron from MKS instruments). Following H_2 exposure, the chamber was pumped back down to 9×10^{-7} Torr, and the hydrogenation cycle was repeated with the next sequential gas pressure, until reaching the 13.33 kPa limit.

The relationship between the mass gained by the QC, Δm, due to the H_2 adsorption of the purified MWCNTs and the shift of the resonance frequency of the QC, Δf_m, can be expressed by Eq. (1), Sauerbrey equation [39, 40, 41]:

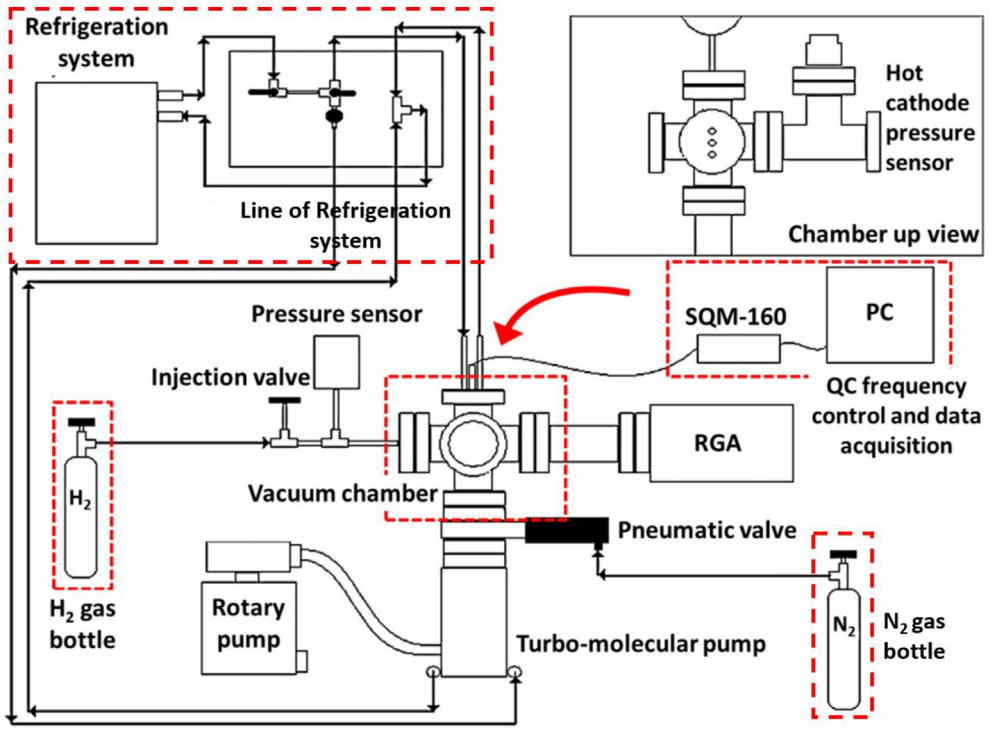

Figure 2. Scheme of the experimental set up for the H_2 adsorption studies.

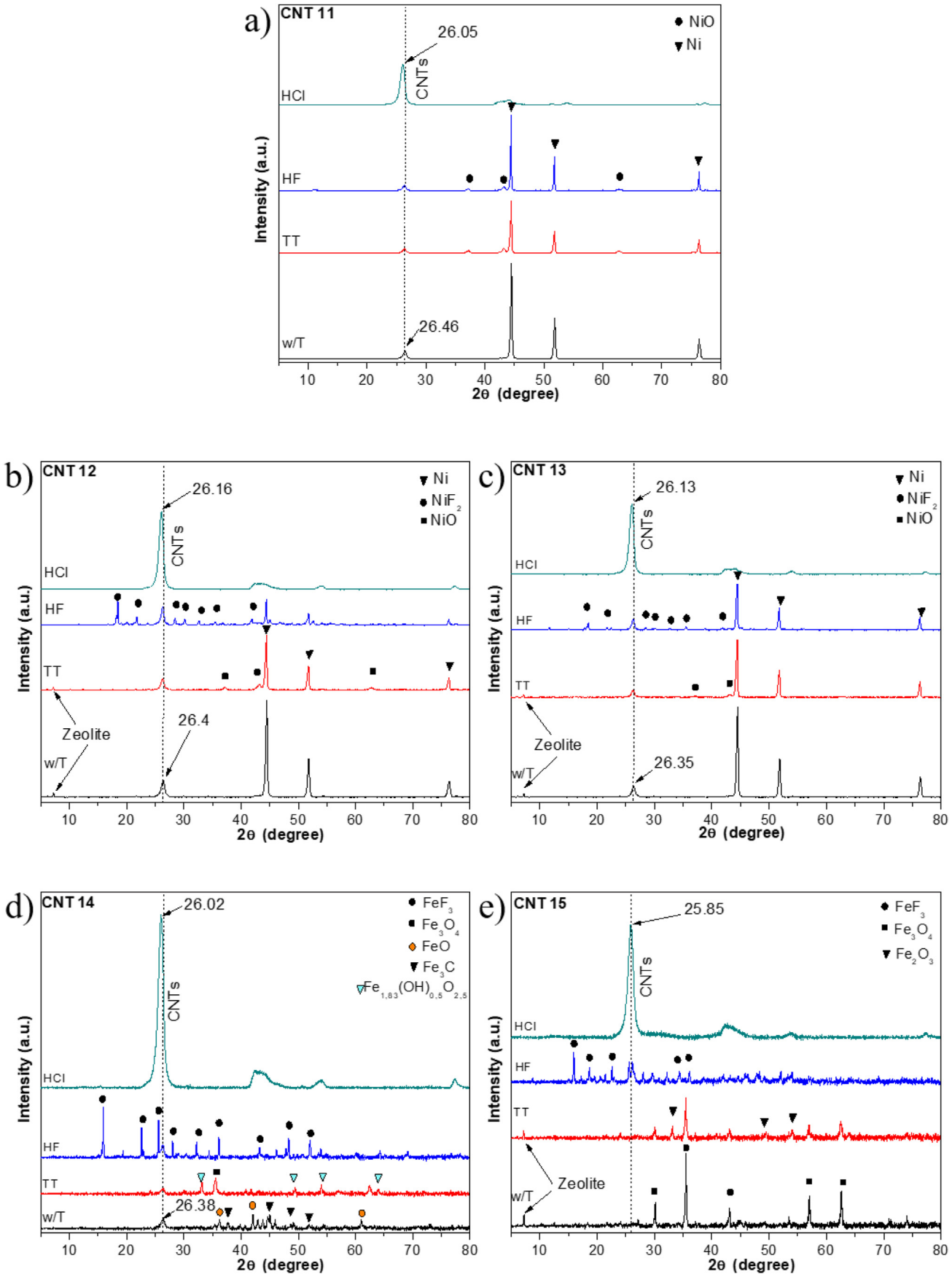

Figure 3. XRD patterns of MWCNTs during the purification process: a) CNT11, b) CNT12, c) CNT13, d) CNT14, and e) CNT15).

Table 3. Surface and Raman characteristics of purified multi-walled carbon nanotubes.

Purified Samples	SSA (m^2 g^{-1})	Average pore diameter (nm)	Intensity ratio (unpurified) (I_D/I_G)	Intensity ratio (purified) (I_D/I_G)
CNT11	68.7 ± 0.2	13.9	1.02	0.78
CNT12	43.6 ± 0.1	17.3	0.77	0.90
CNT13	12.2 ± 1.0	37.9	0.63	0.69
CNT14	53.6 ± 0.2	17.5	0.97	0.71
CNT15	729.4 ± 2.8	22.3	0.95	0.61

$$\Delta f_m = -\frac{2f_0^2}{A\sqrt{\rho \times \mu}}\Delta m \quad (1)$$

where f_o is the unloaded-QC resonant frequency, ρ is quartz density, μ is the bulk modulus of the AT-cut QC and A is the area covered by the mass. This equation indicates that a negative variation of the resonance frequency corresponds to a gain in mass. However, other factors besides the deposited or adsorbed mass on the QC can affect the resonance frequency of the crystal. In general, the total measured, QC resonance frequency change, ΔF, can be expressed as in Eq. (2):

$$\Delta F = \Delta f_m + \Delta f_T + \Delta f_P + \Delta f_\mu + \Delta f_R \quad (2)$$

where Δf_P is a function of the gas pressure, Δf_T is a term dependent on the crystal temperature, Δf_μ is related with the density and viscosity of the gas, and Δf_R is associated with surface roughness [42]. The relevance of these different terms in the context of the present work was assessed as follows. First, the effect of temperature on the QC's resonance frequency was minimized by using a water-cooling system (see Figure 2) to maintain the crystal at a temperature of 20 °C and thus the Δf_T term was deemed as negligible. Second, in order to reduce the influence of the H_2 gas pressure, density and viscosity (Δf_P and Δf_μ terms), a bare QC was exposed to H_2 in the experiment pressure range (0.39–13.33 kPa) and its resonance frequency change calculated for each exposure pressure. Third, the roughness term Δf_R was not considered in our calculations (more details below in the Discussion section). Finally, the frequency shifts associated to the adsorbed gas mass, Δf_m, was calculated by subtracting, for each exposure pressure, the blank QC's resonance frequency shifts from the total shift ΔF of the MWCNT-loaded crystals. Similar methods based on comparing a reference bare crystal to a sample-loaded one have been followed in the literature for measuring gas mass adsorption by various materials [43, 44, 45, 46].

3. Results and analysis

3.1. Characterization of purified MWCNTs

In order to investigate the degree of hydrogen storage of purified multi-walled carbon nanotubes (MWCNTs) and their performance on gas adsorption/desorption cycles, MWCNTs were synthesized by AACVD [15, 16] and then purified using thermal treatment and acid treatments, as is shown in Figure 1. After thermal purification process, the weight loss was calculated between initial mass and final mass, where the variation in mass is important because there is a relationship with amorphous carbon or a graphitic weak bond present in each sample. Consequently, a small weight loss was found, less than 1.5 % for samples: CNT11, CNT13, CNT14, and CNT15, respectively; instead, for CNT12 the weight loss was 7.91 %. The results are shown in Table 2.

During the purification procedure, X-ray diffraction (XRD) was used to study the impurities phases present in the samples. XRD results are shown in Figure 3. In all samples, the peak assigned to graphitic structure was observed at approximately $2\theta = 26°$, which is associate with the graphitic plane (0 0 2) or the wall-to-wall distance in MWCNTs [16, 47]. Before and during the purification process, the XRD patterns exhibited the presence of the catalytic and support (w/T), as well as the appearance of new oxidized species due to thermal treatment (TT) and to the acid treatment (HF, HCl) (see Figure 3). Using the assigned value of 2θ for the diffraction plane (0 0 2), the associated interplanar distance (d_{002}) was determined by the Bragg's law [48], which is expressed in Eq. (3):

$$n\lambda = 2d_{hkl}sin\theta \quad (3)$$

where n is an integer associated to the order of the diffraction peak, λ is the wavelength of CuKα radiation (0.154 nm), and d_{hkl} is the interplanar distance with (hkl) Miller index. The interplanar distance calculated with Eq. (3) is detailed in Table 1.

All the samples presented chemical modification indicating an improved purification. For example, an oxidative phase (Fe_2O_3) appeared after thermal treatment. In the case of fluorination, it was possible to observe nickel fluoride and iron fluoride. The zeolite disappeared after the process of washing. These XRD results were supported by Raman measurements and TEM images. Finally, the purification process was highly efficient and easy to operate, reducing the presence of impurities.

The N_2 adsorption isotherms (at 77 K) was used to determine the surface characteristics, namely the specific surface area (SSA) and average pore size of the MWCNTs. The results are shown in Table 3. Brunauer–Emmett–Teller (BET) surface analysis [49] of samples showed that the sample CNT15 had the highest SSA, being 10 times higher in comparison with the other samples. Additionally, all samples are mesoporous with sample CNT13 having the biggest average pore size, being followed by sample CNT15. Considering these two aspects of SSA and average pore size, it is possible to propose that the sample CNT15 will exhibit favorable behavior for H_2 adsorption.

Raman spectroscopy is a powerful technique for the characterization of the structure of CNTs and here it is performed to confirm the degree of crystallinity of the samples. Figure 4 shows the Raman spectra of the raw and purified MWCNTs at the 633 nm laser excitation wavelength. As shown in Figure 4a (raw MWCNTs), two distinct peaks were observed at about 1580 and 1327 cm^{-1} corresponding to the high-frequency E_{2g} first-order vibrational mode (G-band (I_G)) and to the disorder (D-band (I_D)) of the graphite structure. Whereas, for the purified carbon nanotubes of Figure 4b, the characteristic G- and D-bands were observed at around 1570 and 1345 cm^{-1}. Hence the purified carbon nanotubes presented a shift of G-band and D-band frequency to higher and lower wavenumber with respect to raw carbon nanotubes. This shift may be attributed to an inter-tube van der Waals interaction [16]. However, when the number of walls increases the inter-tube spacing decreases. Besides, the samples present a lower intensity in the G-band that is comparable with intensity of the D-band, being typical in MWCNTs.

On the other hand, the intensity ratio (I_D/I_G) is indicative of the crystallinity of the carbon nanotubes [15, 16, 50, 51], where values closer to one indicate more defects contained in the graphene wall and the presence of a lower degree of crystallinity of the carbonaceous material [15, 52]. From the Raman spectra in Figure 4, Table 3, and I_D/I_G ratio, it is observed that the samples present a low degree of crystallinity, as well as defects contained in graphene walls of the nanotubes. As shown in Figure 4b, these characteristic vibrational modes in the Raman spectra are still present after acid treatments. Furthermore, it is observed that for purified carbon nanotubes, the ratio I_D/I_G decreases for CNT11, CNT14, and CNT15 and increases for CNT12 and CNT13 as compared to unpurified MWCNTs. Thus, defects are still

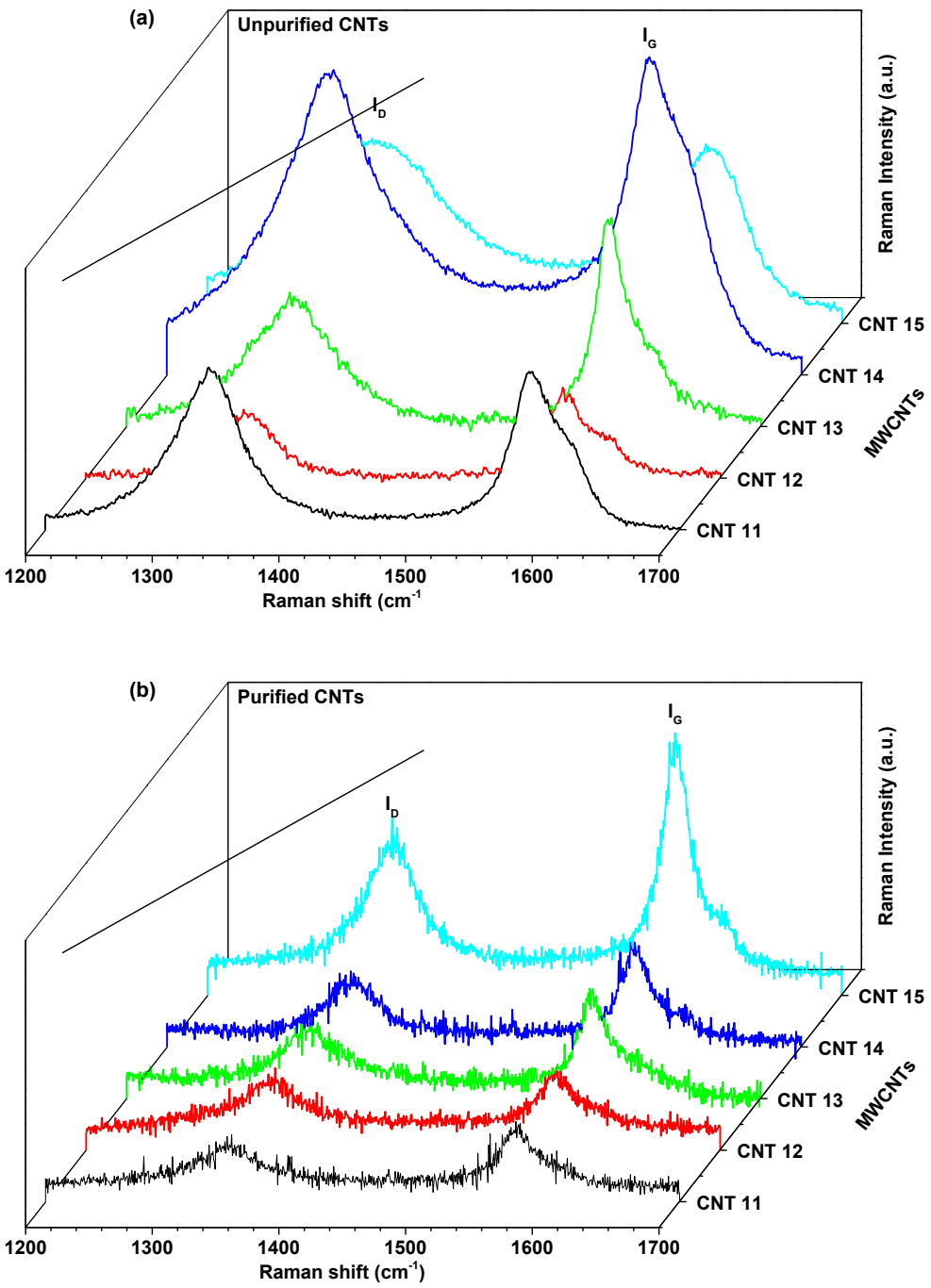

Figure 4. Raman spectra of the (a) as grown and (b) purified MWCNTs.

present in the purified samples. These may adsorb hydrogen molecules more selectively in contrast to the ideal hexagonal structures of CNTs [8]. The Raman results are in good agreement with our XRD results and the morphologies observed in the TEM analysis, where all samples presented chemical and structural modification after purification stage. In addition, small loss mass and the absence of impurities content indicate the purity of CNTs.

Figure 5 shows TEM and HRTEM images of purified MWCNTs. Figure 5(a)–(c) show images of straight carbon nanotube (CNT12). From Figure 5(c) can be seen that there is no catalyst present at the tip of the nanotube, and it is found to be broken. Using the interplanar distance (d_{002}) from XRD, the number of nanotubes was estimated. Figure 5(b) shows that the CNT12 sample has ~48 concentric carbon nanotubes. While Figures 5(d) and (e), the MWCNTs (CNT15) present a very different morphology due to that the sample grew under different synthesis conditions, using magnetite (at 90%) and zeolite-like support and under an Ar flow. Additionally, the CNT15 sample displayed ~115 concentric carbon nanotubes. Also, there is no catalyst present in the carbon nanotubes, only with some defects seen in the graphite layers. Furthermore, the outer surface of the tube wall is free of amorphous carbon layer.

3.2. Adsorption kinetics and H_2 storage capacity of purified MWCNTs

3.2.1. Gas adsorption kinetics under hydrogenation cycles

To study the H_2 adsorption kinetics and storage capacities of the MWCNT samples, a quartz crystal microbalance (QCM) system was used, following the procedure described in the 2.4 section.

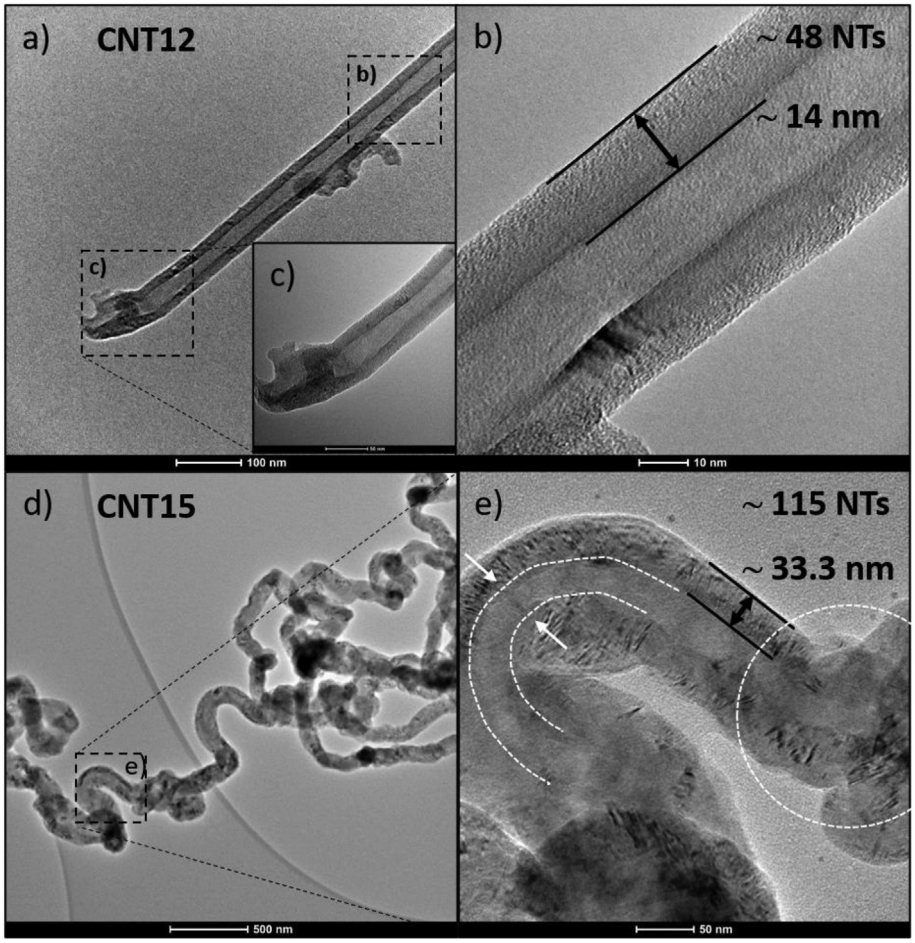

Figure 5. TEM images of the purified sample (a–c) CNT12 and (d–e) CNT15. (b–c) Zoom of the dotted frame in (a), showing the tips and walls of the purified CNT12. (e) The dotted frame in (d) with increased magnification shows the curved tubing, the wall, and defects in purified CNT15.

Figure 6 shows four representative curves of the H_2 exposure and adsorption process (acquired from sample CNT13), as determined by the changes of the QC resonance frequency in real-time. Three different stages are observed: (a) the resonance frequency of the QC while in vacuum of $\sim 1.19 \times 10^{-7}$ kPa (base frequency), (b) a spike on the resonance frequency caused by the injection of H_2 at around 60 s and an immediate drop in the resonance frequency, and (c) a region with a relatively stable resonance frequency (final frequency). The difference between the final and base resonance frequencies is substituted into Sauerbrey's equation (see Eq. (1)) for calculating the gas adsorption capacities, while considering the correction term described in 2.4 section.

With respect to the adsorption kinetics, it is seen in Figure 6(a) that the resonance frequency shows a decreasing trend during the whole H_2 exposure time (between the 60 and 480 s), without reaching a clear saturation condition. On the contrary, the curves shown in Figure 6(b) display a faster decrease in the resonance frequency after the gas injection, and then a small positive slope during the rest of the H_2 exposure. Due to these differences in the adsorption behavior at different pressures, the adsorption kinetics were studied by estimating the time required by the samples to reach a 95 % of the total H_2 adsorption ($t_{95\%}$) as obtained under a certain pressure during the 7 min that lasts the gas exposure. The obtained $t_{95\%}$ values were plotted as a function of H_2 pressure, as shown in Figure 7, and error bars were estimated based on the time required to reach the different H_2 pressures by means of the injection valve (Figure 2). This is because in general a higher pressure requires longer injection times; the longest injection time measured was selected for the error estimation to reduce the influence of possible variations in the manually driven gas injection process. From Figure 7, samples CNT11, CNT12, CNT13 and CNT15 present a similar trend in their $t_{95\%}$ curves: higher H_2 exposure pressures tend to increase the H_2 adsorption speed, which means lower $t_{95\%}$ time values. In general, for this set of samples, after 1.99 kPa of exposure pressure only slight differences in $t_{95\%}$ are observed, where practically the H_2 adsorption process occurs between 29 and 55 s depending on the type of sample, as established in Figure 7. In contrast, sample CNT14 (Figure 7(b)) presents a different behavior, starting with a decrease in $t_{95\%}$ for exposure pressures between ~ 0.39 and ~2.66 kPa (first and fourth hydrogenation cycle, respectively), with an abrupt increase on $t_{95\%}$ for the ~3.07 kPa exposure pressure (fifth cycle). Finally, it shows a new decrease on the $t_{95\%}$ value over the last four H_2 exposures. In general, it was found that the adsorption kinetics accelerate with increasing the H_2 pressure, up to 2.66 kPa. This assumption is based on the fast response exhibited by the bare QCs when exposed to different types of gases (H_2, CO_2, CO) and pressures (results not shown here). The bare QCs have response times that are one order of magnitude shorter than those loaded crystals.

3.2.2. *Hydrogen storage capacity under increasing exposure pressures*

The H_2 adsorption capacities of the purified MWCNT are shown in Figure 8. For comparison purpose, previously reported H_2 adsorption data for unpurified samples CNT11 to CNT14 [15,16] have been included. From Figure 8 and focusing on the purifies samples, only sample CNT15 displayed an H_2 adsorption capacity above the 1.0 wt%, while the rest of samples did not cross this threshold. A maximum adsorption capacity of 3.4 wt% was achieved by sample CNT15 at an H_2 pressure of 5.73 kPa. The maximum adsorption capacities achieved by each sample are summarized in Table 4, indicating also the corresponding H_2 exposure pressure at

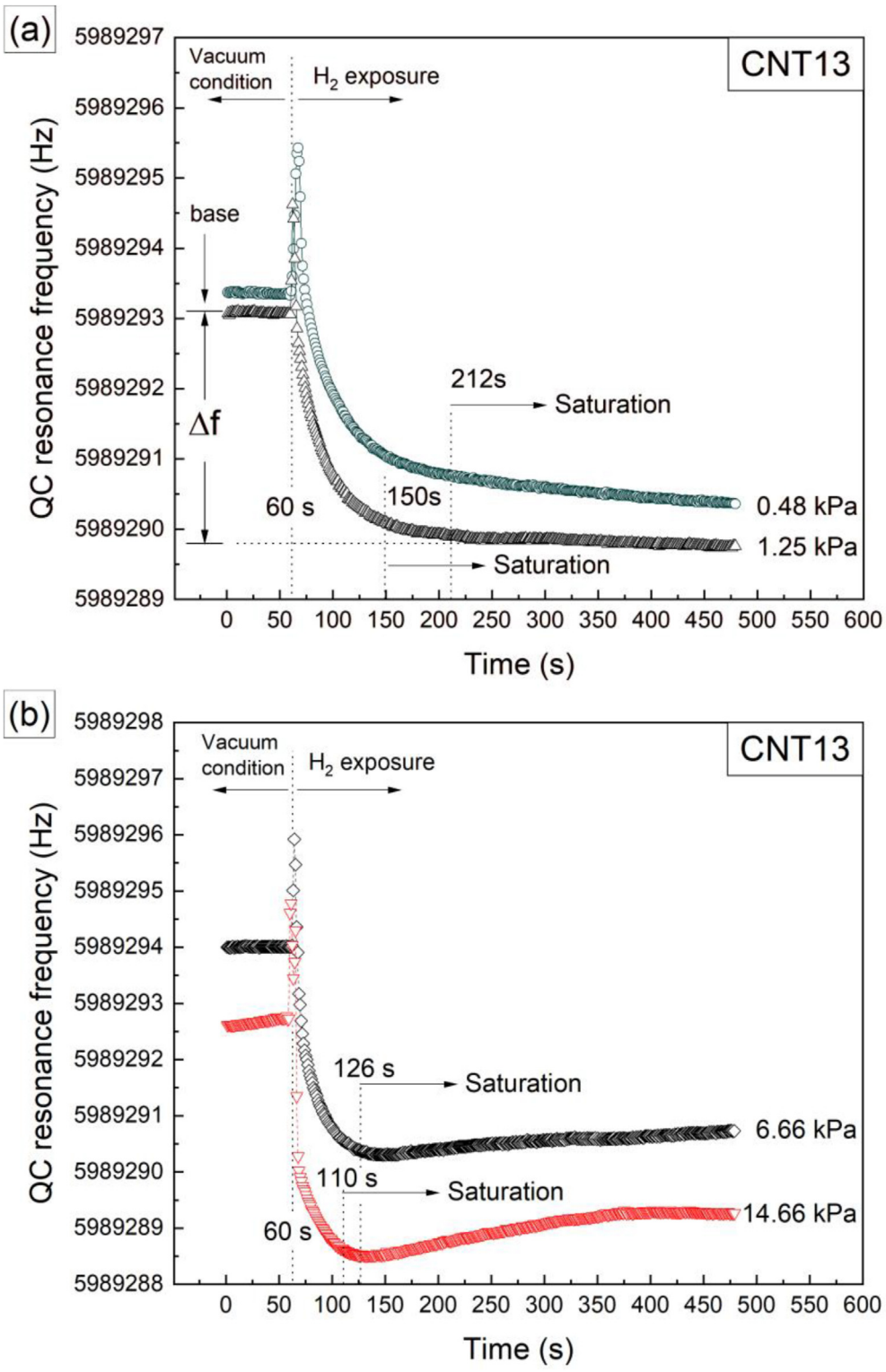

Figure 6. (a–b) Representative curves of the H_2 adsorption kinetics represented by the changes of the QC resonance frequency as a function of time monitored in-situ while the sample (CNT13) was underwent under successive hydrogenation cycles with increasing exposure pressures. (a) Under pressures of 0.48 and 1.25 kPa and (b) under higher exposure pressures of 6.66 and 14.66 kPa.

which each capacity was reached. Interestingly, it was found that purification decreased the H2 adsorption on samples CNT11 to CNT14, contrary to what was observed in sample CNT15. This observation will be commented in the discussion section.

Finally, to test the stability of the measured H_2 capacity of samples CNT15, a repetition test was carried out on over a year after the first measurements. The obtained results are presented in Figure 9, where the dotted line marks the maximum H_2 adsorption capacity of the other CNT samples beside CNT15. As shown in this figure, sample CNT15 reached a peak adsorption capacity of around 3.3 wt% but exhibited a slight decrease in its H_2 adsorption capacity

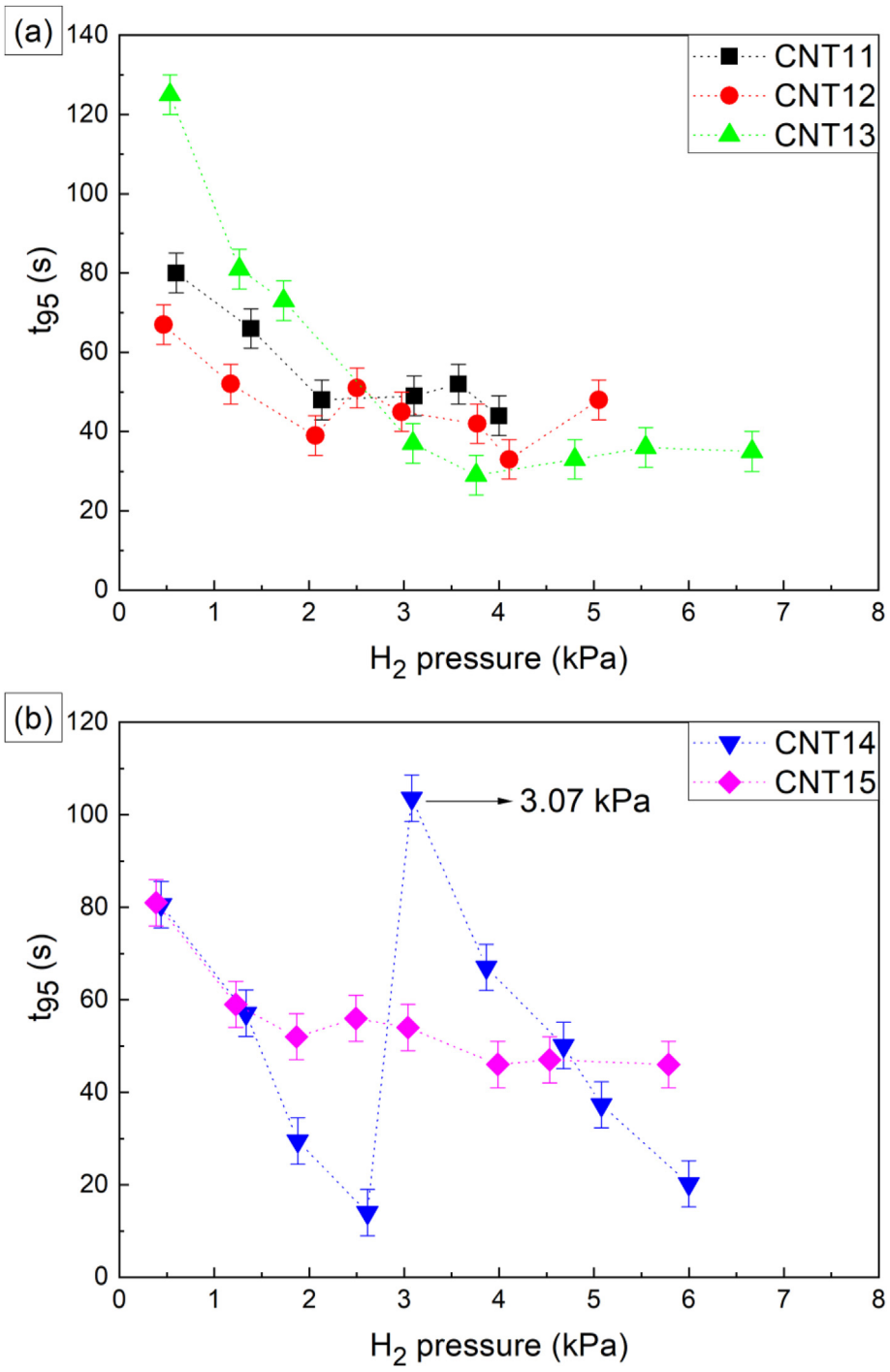

Figure 7. (a–b) Kinetics curves for $t_{95\%}$ versus H_2 exposure pressure for samples (a) CNT11, CNT12 and CNT13 which used Ni Catalyst, and (b) CNT14 and CNT15 grown with magnetite catalyst.

with increasing pressures. However, the measured H_2 adsorption capacity of CNT15 remained higher than of the others CNT samples.

3.2.3. *Performance on reversibility of H_2 loading/unloading process*

Another relevant aspect for hydrogen storage by low pressure sorption is the stability of the sorbent during cycles of H_2 loading and unloading. In this work, the stability of the purified MWCNTs was evaluated by comparing the measured base resonance frequency of the loaded QCs for each specific hydrogenation step, with the initial value obtained before the first H_2 exposure. For example, a stable base frequency is an indicator of a good capacity to release the adsorbed H_2.

The results obtained from the base resonance frequency comparison are summarized in Figure 10, where $\Delta f_n = f_B^n - f_B^1$, with f_B^n and f_B^1 corresponding to the base resonance frequency of the n^{th} and first hydrogenation steps, respectively. Here it is observed that three samples (CNT11, CNT13 and CNT15) exhibited a better stability across the successive hydrogenation steps, with variations in the base resonance frequency of less than ±2 Hz. Among the group of the more stable samples, CNT15 stands out as the one with the flatter Δf_B curve. On the other hand, the remaining two samples, CNT12 and CNT14, exhibited important variations on their base resonance frequency between the different hydrogenation steps.

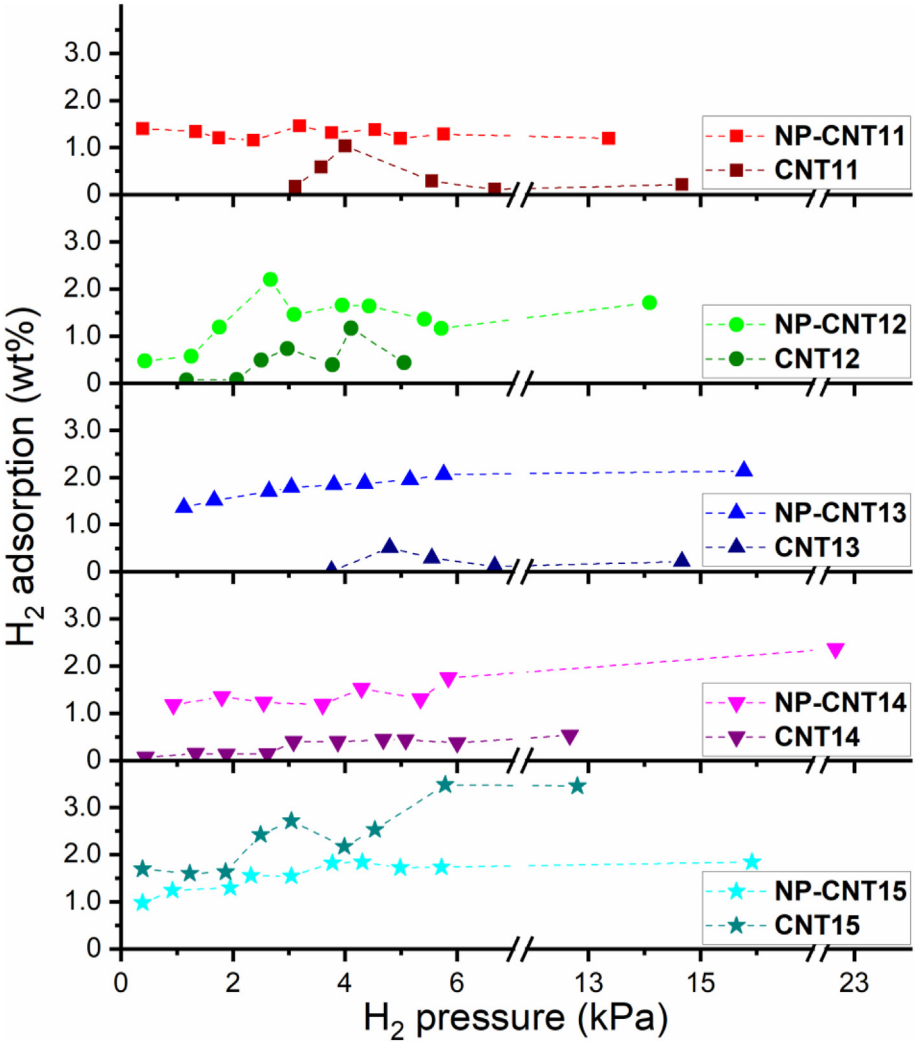

Figure 8. H_2 storage capacity at RT as a function of the gas exposure pressure from the purified (CNT#) and the unpurified (NP-CNT#) MWCNTs.

Table 4. Maximum values of H_2 adsorption reached by the purified MWCNTs under the indicated exposure pressures.

Purified Samples	H_2 Adsorption Maximum (wt%)	Exposure Pressure (kPa)
CNT11	1.04	**3.99**
CNT12	1.17	**4.13**
CNT13	0.51	**4.79**
CNT14	0.54	**12.66**
CNT15	3.48	**5.73**

4. Discussion

4.1. Hydrogen adsorption kinetics

The gas adsorption kinetics during the first hydrogenation cycles, up to 2.66 kPa of exposure, is a slightly dependent on the morphological and structural characteristics of the purified carbon nanotubes (MWCNTs). This dependency is seen in Figure 7, where the $t_{95\%}$ value is different for every sample at this low-pressure range. However, it is not possible in this work to correlate the adsorption kinetics with some characteristic of the MWCNTs, such as density or crystallinity defects, specific surface area or size of the nanotubes. In spite of this, our study on purified MWCNTs revealed that the hydrogen adsorption kinetics, represented by the $t_{95\%}$ value, does not present fluctuations as pronounced at higher exposure pressures, i.e., above 2.66 kPa (see Figure 7), for the different types of MWCNTs. The exception here is the CNT 14 sample which exhibited an anomalous behavior, as shown in Figure 7b. This means that the structural and morphological characteristics of the purified MWCNTs do not seem to be that important on the adsorption kinetics at this higher-pressure range (> 2.66 kPa). From Figure 7 it is seen that, regardless of sample type, the $t_{95\%}$ values for this pressures range remain between 30 and 50 s approximately.

4.2. Hydrogen storage capacity

It was mentioned in the previous section that sample CNT15 showed the highest H_2 adsorption capacity in the range of H_2 pressures studied, with a maximum value of 3.48 wt% for the higher pressures of 5.33 and 13.33 kPa; this is at least three times higher than the values obtained for the rest of the MWCNT samples. The H_2 adsorption capacity of SWCNT and MWCNT depends on various factors, such as the tubes morphological characteristics, the SSA, and defects density, for example. In our case, the sample CNT15 exhibited distinctive morphological characteristics such as larger nanotube diameters and a higher number of concentric nanotubes (~115 NTs), along with the highest SSA of ~730 $m^2\ g^{-1}$. With

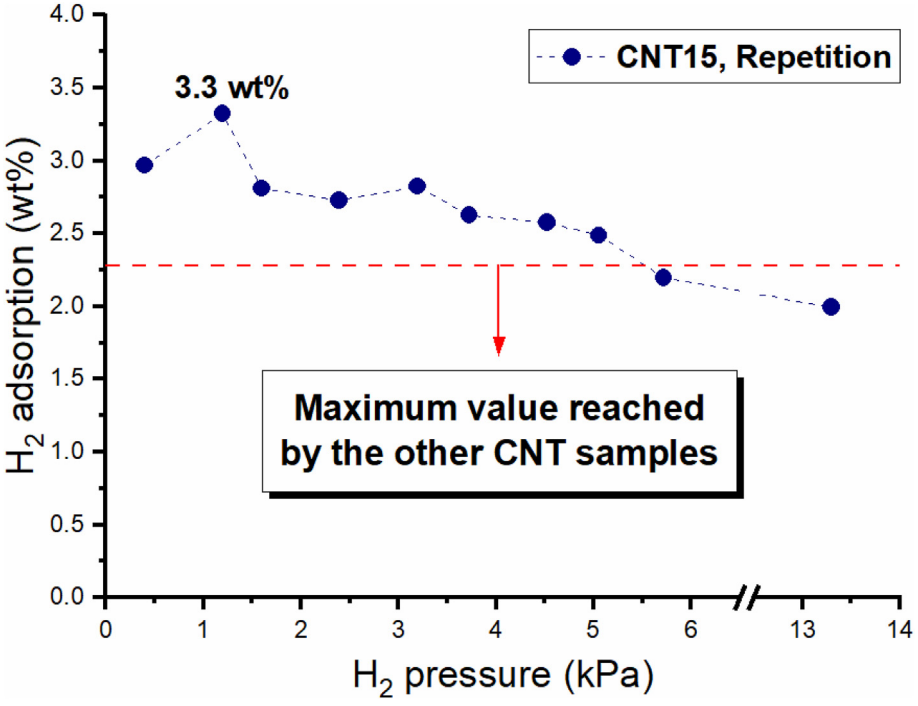

Figure 9. Repetition of the RT H_2 adsorption capacity measurement of sample CNT15, carried over a year after the first measurements.

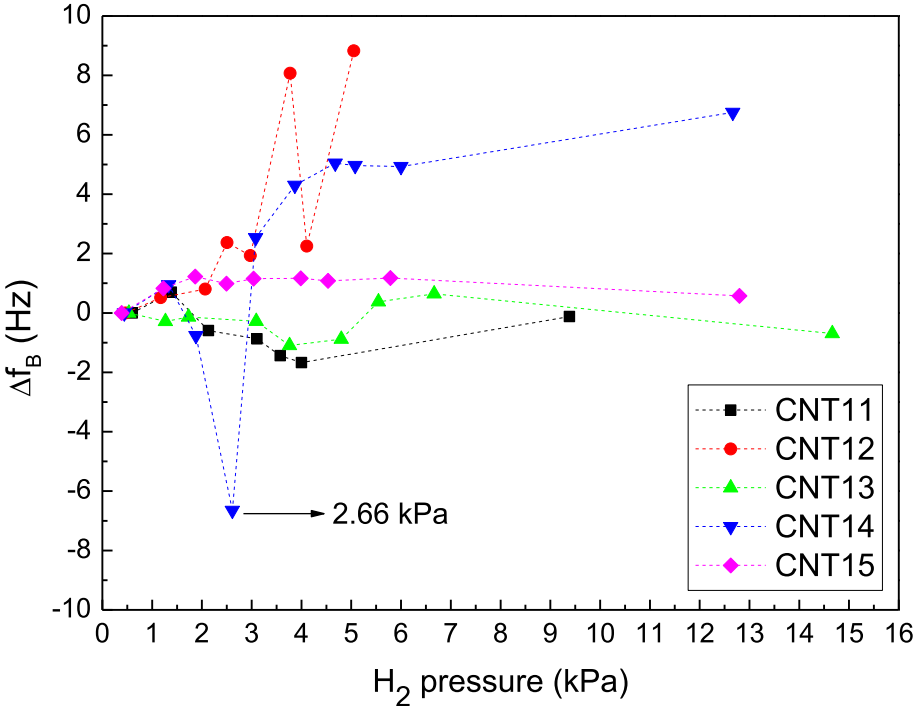

Figure 10. Shift of the base QC resonance frequency with respect to the value registered in the first hydrogenation cycle as a function of the H_2 exposure pressure determined for all the samples.

respect to defects density, the purified sample CNT15 shows the lowest value of I_D/I_G in Raman spectroscopy, which suggests higher crystallinity and lower defect content. However, it still shows defects within the concentric walls of the nanotube (~115 NTs). Such defects contribute to the increase the SSA, providing more adsorption sites.

Furthermore, it has been reported that H_2 adsorption capacity of CNTs could be correlated with the SSA obtained from N_2 adsorption isotherms [53, 54]. Similarly, Elyassi et al. [55] found that both a high SSA and a high fractional content of micro pores (alongside with defects) are relevant for H_2 adsorption. On the other hand, it has been found that an increase in SSA can be followed by a decrease in the H_2 adsorption capacity. Sami Ullah Rather [56] found that acid purification of MWCNTs doubled the SSA of the nanotubes but H_2 adsorption capacity decreased by around 10%, and author suggested that the loss in H_2 adsorption was

mainly due to the removal of metallic catalyst residues. Similarly, Ioannatos and Verykios [57] studied different types of CNTs (MWCNTs and SWCNTs) and found that, on a H_2 volume per area basis, nanotubes with larger SSAs adsorbed lower volumes of H_2 and that an opposite trend was observed when comparing the different types of CNTs on a weight basis. Furthermore, in Ref [57], an increase on H_2 adsorption with increasing CNTs purity was observed, effect that was explained in terms of an increase of available adsorption sites after purification.

Considering this context and the available characterization data for our samples, it can be argued that the higher H_2 adsorption capacity of sample CNT15 is linked to its high SSA, which should be due to a relatively higher content of micro pores (beneficial for H_2 adsorption), allowing to counteract the negative impact of having a lower defect concentration (according to Raman results) that might work as adsorption sites for H_2. Finally, the potentially negative effect on H_2 adsorption of removing catalyst particles is again counteracted by the high SSA of purified sample CNT15, while for the rest of the purified CNT samples, their low SSA after purification is not enough for this and thus their H_2 adsorption capacity decreases.

4.3. Hydrogen adsorption mechanisms

At first sight it may appear that the structural and morphological characteristics of the CNT15 sample are enough to support its high H_2 adsorption value of 3.48 wt%. Other factors should be evaluated before concluding that these physical characteristics are enough to justify this high value. One is that the possible hydrogen adsorption mechanisms on carbon nanotubes play an important role. Considering a simple geometric model, the commensurate physisorption of a monolayer of spherically-shaped hydrogen molecules with a kinetic diameter of 2.9 Å on a $\sqrt{3}x\sqrt{3}$ bidimensional graphene superlattice [58] would cause a H:C ratio of 1:3. Moreover, considering that the mass ratio between one hydrogen atom and one carbon atom is 1:12, the H_2 adsorption capacity of this graphene layer would be of ~2.8 wt% for a commensurate monolayer of hydrogen molecules [59]. This simple geometric argument indicates that for reaching higher values of H_2 adsorption on graphene layers of carbon nanotubes other mechanisms are participating. Dillon et al. [24] investigated the hydrogen adsorption capacity on single wall carbon nanotubes (SWCNTs) using temperature-programmed desorption (TPD) measurements. They suggested that the hydrogen molecules can access and accumulate inside the tubes if these have open tube tips. On producing samples with a high concentration of short SWCNTs with open ends, they determinate a hydrogen adsorption of this type of nanotubes of about 4 wt% at room temperature and 66.66 kPa H_2 exposure pressure. In addition, they concluded that most of hydrogen molecules are stored within the capillary, as opposed to the interstitial spaces between nanotubes. In this sense and, as revealed by the TEM images of the CNT15 sample, no catalyst is found at the tip of the purified nanotubes, this fact together greater inner diameters of this sample would favor the access of the hydrogen molecules towards the inner core of the MWCNTs and the possible filling of the capillaries [60]. On the other hand, the morphological characteristics of the nanotubes present in the CNT15 sample (see Figure 5) allow the possibility of providing a lot of interstitial spaces, when agglomerated. However, the confirmations of this adsorption mechanism hypothesis require further research.

In summary, in spite of the absence of costly precious metals, such as Au or Pd, the CNT15 sample with its high H_2 adsorption capacity, close to 3.5 wt% and good recovery during H_2 adsorption/desorption cycles, make it a clear candidate for H_2 adsorption and storage applications.

5. Conclusions

In this work significant improvement in hydrogen storage capacities has been achieved using purified MWCNTs. XRD analysis confirms that metallic catalyst and amorphous carbon in purified MWCNTs were removed and dissolved by a thermal treatment followed by an acid process. The greatest SSA obtained was for the sample CNT15, whose value was 10 times higher than other samples. Raman measurements and TEM analysis showed that the obtained carbon nanotubes (MWCNT) have some defects and a certain degree of crystallinity in the graphite layers. It was also observed that the purified MWCNTs (i.e., CNT15) presents excellent characteristics for H_2 adsorption because it can adsorb more hydrogen molecules in comparison to ideal hexagonal structures of CNTs. Additionally, the morphology of the nanotubes depends on the synthesis conditions and purification procedure.

The hydrogen adsorption capacity of purified MWCNTs was studied with a QCM. Purified MWCNTs (such as CNT15) show higher H_2 adsorption capacity than unpurified MWCNTs. The best result of H_2 storage capacity was found to be 3.48 wt% at 12.79 kPa of H_2 exposure pressure at room temperature. However, the H_2 storage capacity of pure carbonaceous materials at ambient temperature and pressure is still well below the benchmarking set by the U.S. Department of Energy (DOE) for stationary and portable applications and remains a significant challenge for transportation targets.

Declarations

Author contribution statement

Edgar Mosquera-Vargas: Conceived and designed the experiments; Performed the experiments; Analyzed and interpreted the data; Contributed reagents, materials, analysis tools or data; Wrote the paper.

Rocío Tamayo, Martín Roble: Performed the experiments; Wrote the paper.

Mauricio Morel, Donovan E. Díaz-Droguett: Conceived and designed the experiments; Performed the experiments; Analyzed and interpreted the data; Wrote the paper.

Funding statement

This work was supported by Chilean Government (FONDEF ID14i10124, CONICYT-PIA ACT1409, PAI7190056), Colombian Government (Minciencias BPIN 2020000100377) and Universidad del Valle – Colombia (Strengthening of Centers and Institutes). D.E. Diaz-Droguett was supported by the II190019 Interdisciplinary Project (2019) of the VRI-PUC and the Energy Interdisciplinary Project (2019) from the Energy Research Center of PUC Chile. M. Roble was supported by the Doctoral Grant from ANID-Chilean Government.

Data availability statement

Data included in article/supplementary material/referenced in article.

Declaration of interests statement

The authors declare no conflict of interest.

Additional information

No additional information is available for this paper.

Acknowledgements

The authors thank PUC-Chile and the University of Chile for providing their facilities and equipment for this research. The authors especially thank the contribution of Edmund Wyndham for comments in the manuscript.

References

[1] Organization for economic cooperation and development energy: the next fifty years, in: OECD (Ed.), The Long-Term Future for Energy: an Assessment of Key Trends and Challenges, OECD Publications, Paris, 2019, pp. 7–17.
[2] M. Sankir, N.D. Sankir, Hydrogen Storage Technologies, first ed., John Wiley & Sons. Inc, New York, 2018. Scrivener Publishing LLC, Massachusetts.
[3] M. Mohan, V.K. Sharma, E.A. Kumar, V. Gayathri, Hydrogen storage in carbon materials–A review, Energy Storage 1 (2019) 1–26.
[4] A.D. Franklin, The road to carbon nanotube transistors, Nature 489 (2013) 443–444.
[5] J.T.-W. Wang, L. Cabana, M. Bourgognon, H. Kafa, A. Protti, K. Venner, A.M. Shah, J.K. Sosabowski, S.J. Mather, A. Roig, X. Ke, G. Van Tendeloo, R.T.M. de Rosales, G. Tobias, K.T. Al-Jamal, Magnetically decorated multiwalled carbon nanotubes as dual MRI and SPECT contrast agents, Adv. Funct. Mater. 24 (2014) 1880–1894.
[6] A. Ahmed, S. Seth, J. Purewal, A.G. Wong-Foy, M. Veenstra, A.J. Matzger, D.J. Siegel, Exceptional hydrogen storage achieved by screening nearly half a million metal-organic frameworks, Nat. Commun. 10 (2019) 1568.
[7] Y. Li, H. Liu, Grand canonical Monte Carlo simulation on the hydrogen storage behaviors of the cup-staked carbon nanotubes at room temperature, Int. J. Hydrogen Energy 46 (2021) 6623–6631.
[8] A. Reyhani, S.Z. Mortazavi, S. Mirershadi, A.Z. Moshfegh, P. Parvin, A. Nozad, Hydrogen storage in decorated multiwalled carbon nanotubes by Ca, Co, Fe, Ni, and Pd nanoparticles under ambient conditions, J. Phys. Chem. C 115 (2011) 6994–7001.
[9] K.-S. Lin, Y.-J. Mai, S.-R. Li, C.-W. Shu, C.-H. Wang, Characterization and hydrogen storage of surface-modified multiwalled carbon nanotubes for fuel cell application, J. Nanomater. 2012 (2012) 1–12.
[10] S.L. Katar, D. Hernández, A. Biaggi-Labiosa, E. Mosquera-Vargas, L. Fonseca, B.R. Weiner, G. Morell, SiN/bamboo like carbón nanotube composite electrodes for lithium ion rechargeable batteries, Electrochem. Acta 55 (2010) 2269–2274.
[11] S. Iijima, Helical microtubules of graphitic carbon, Nature 354 (1991) 56.
[12] C. Liu, Y. Chen, C.-Z. Wu, S.-T. Xu, H.-M. Cheng, Hydrogen storage in carbon revisited, Carbon 48 (2010) 452–455.
[13] H.-M. Cheng, Q.-H. Yang, C. Liu, Hydrogen storage in carbon nanotubes, Carbon 39 (2001) 1447–1454.
[14] S. Banerjee, S. Murad, I.K. Puri, Hydrogen storage in carbon nanostructures: possibilities and challenges for fundamental molecular simulations, Proc. IEEE Inst. Electr. Electron. Eng. 94 (10) (2006) 1806–1814.
[15] E. Mosquera, D.E. Diaz-Droguett, N. Carvajal, M. Roble, M. Morel, R. Espinoza, Characterization and hydrogen storage in multi-walled carbon nanotubes grown by aerosol-assisted CVD method, Diam. Relat. Mater. 43 (2014) 66–71.
[16] M. Morel, E. Mosquera, D.E. Diaz-Droguett, N. Carvajal, M. Roble, V. Rojas, R. Espinoza-González, Mineral magnetite as precursor in the synthesis of Multi-Walled Carbon Nanotubes and their capabilities of hydrogen adsorption, Int. J. Hydrogen Energy 40 (2015) 15540–15548.
[17] G.E. Froudakis, Hydrogen storage in nanotubes and nanostructures. Mater, Today Off. 14 (2011) 324–328.
[18] DoE office of energy efficiency and renewable energy, Hydrogen Storage. Available from: http://energy.gov/eere/fuelcells/hydrogen-storage.
[19] B. Panella, M. Hirscher, R. Siegmar, Hydrogen adsorption in different carbon nanostructures, Carbon 43 (2005) 2209–2214.
[20] V.K. Sharma, E.A. Kumar, Metal hydrides for energy applications-classification, PCI characterization and simulation, Int. J. Energy Res. 14 (2016) 901–923.
[21] K. Spyrou, D. Gournis, P. Rudolfa, Hydrogen storage in graphene-based materials: efforts towards enhanced hydrogen absorption, ECS J. Solid State Sci. Technol. 2 (2013) M3160–M3169.
[22] S.H. Aboutabeli, S. Aminorroaya-Yamini, I. Nevirkovets, K. Konstantinov, H.K. Liu, Enhanced Hydrogen storage in graphene oxide-MWCNTs composite at room temperature, Adv. Energy Mater 2 (2012) 1439–1446.
[23] H. Jeing, Y. Feng, M. Chen, Y. Wang, Synthesis and hydrogen-storage performance of interpenetrated MOF-5/MWCNTs hybrid composite with high mesoporosity, Int. J. Hydrogen Energy 38 (2013) 10950–10955.
[24] A.C. Dillon, K.M. Jones, T.A. Bekkedahl, C.H. Kiang, D.S. Bethune, M.J. Heben, Storage of hydrogen in single-walled carbon nanotubes, Nature 386 (1997) 377–379.
[25] C.P. Deck, K. Vecchio, Prediction of carbon nanotube growth success by the analysis of carbon–catalyst binary phase diagrams, Carbon 44 (2006) 267–275.
[26] S. Esconjauregui, C.M. Whelan, K. Maex, The reasons why metals catalyze the nucleation and growth of carbon nanotubes and other carbon nanomorphologies, Carbon 47 (2009) 659–669.
[27] H. Liu, D. Tagaki, S. Chiashi, T. Chokan, Y. Homma, Investigation of catalytic properties of Al2O3 particles in the growth of single-walled carbon nanotubes, J. Nanosci. Nanotechnol. 10 (2010) 4068–4073.
[28] S.A. Steiner, T.F. Baumann, B.C. Bayer, R. Blume, M.A. Worsley, W.J. MoberlyChan, E.L. Shaw, R. Schlögl, A.J. Hart, S. Hofmann, B.L. Wardle, Nanoscale zirconia as a nonmetallic catalyst for graphitization of carbon and growth of single- and multiwall carbon nanotubes, J. Am. Chem. Soc. 131 (2009) 12144–12154.
[29] J.J. Liang, Y. Huang, J. Oh, M. Kozlov, D. Sui, S.L. Fang, R.H. Baughman, Y.F. Ma, Y.S. Chen, Electromechanical actuators based on graphene and graphene/Fe3O4 hybrid, Adv. Funct. Mater. 21 (2011) 3778–3784.
[30] C.Y. Hou, Q.H. Zhang, M.F. Zhu, Y.G. Li, H.Z. Wang, One-step synthesis of magnetically-functionalized reduced graphite sheets and their use in hydrogels, Carbon 49 (2011) 47–53.
[31] Y.H. Xue, H. Chen, D.S. Yu, S.Y. Wang, M. Yardeni, Q.B. Dai, M.M. Guo, Y. Liu, F. Lu, J. Qu, L.M. Dai, Oxidizing metal ions with graphene oxide: the in situ formation of magnetic nanoparticles on self-reduced graphene sheets for multifunctional applications, Chem. Commun. 47 (2011) 11689–11691.
[32] J.H. Shen, Y.H. Zhu, K.F. Zhou, X.L. Yang, C.Z. Li, Tailored anisotropic magnetic conductive film assembled from graphene-encapsulated multifunctional magnetic composite microspheres, J. Mater. Chem. 22 (2012) 545–550.
[33] H.K. He, C. Gao, Supraparamagnetic, conductive, and processable multifunctional graphene nanosheets coated with high-density Fe_3O_4 nanoparticles, ACS Appl. Mater. Interfaces 2 (2010) 3201–3210.
[34] M. Kumar, Y. Ando, Chemical vapor deposition of carbon nanotubes: a review on growth mechanism and mass production, J. Nanosci. Nanotechnol. 10 (2010) 3739–3758.
[35] A. Reyhani, S.Z. Mortazavi, A. Nozad Golikand, A.Z. Moshfegh, S. Mirershadi, The effect of various acids treatment on the purification and electrochemical hydrogen storage of multi-walled carbon nanotubes, J. Power Sources 183 (2008) 539–543.
[36] Y. Neslihan, N. Karatepe, Hydrogen storage in single-walled carbon nanotubes purified by microwave digestion method, Int. J. Chem. Mol. Nucl. Mater. Metall. Eng. 5 (7) (2011) 597–602.
[37] M. Chen, H.W. Yu, J.H. Chen, H.S. Koo, Effect of purification treatment on adsorption characteristics of carbon nanotubes, Diam. Relat. Mater. 16 (2007) 1110–1115.
[38] H.Z. Geng, T.H. Kim, S.C. Lim, H.K. Jeong, M.H. Jin, Y.W. Jo, Y.H. Lee, Hydrogen storage in microwave-treated multi-walled carbon nanotubes, Int. J. Hydrogen Energy 35 (2010) 2073–2082.
[39] T.G. Sauerbrey, Verwendug von Schwingquarzen zur Wägung dünner Schichten und zur Microwägung, Z. Phys. 155 (1959) 206–222.
[40] V.M. Mecea, From quartz crystal microbalance to fundamental principles of mass measurements, Anal. Lett. 38 (2005) 753–767.
[41] R. Lucklum, P. Hauptmann, The quartz microbalance: mass sensitivity, viscoelasticity and acoustic amplification, Sensor. Actuator. B Chem. 70 (2000) 30–36.
[42] Y.-T. Wu, P.-J. Akoto-Ampaw, M. Elbaccouch, M.L. Hurrey, S.L. Wallen, C.S. Grant, Quartz crystal microbalance (QCM) in high-pressure carbon dioxide (CO2): experimental aspects of QCM theory and CO2 adsorption, Langmuir 20 (9) (2004) 3665–3673.
[43] B.Y. Wei, M.-C. Hsu, Y.-S. Yang, S.-H. Chien, H.-M. Lin, Gases adsorption on single-walled carbon nanotubes measured by piezoelectric quartz crystal microbalance, Mater. Chem. Phys. 81 (1) (2003) 126–133.
[44] S.C. Lim, K.K. Kim, S.H. Jeong, K.H. An, S.-B. Lee, Y.H. Lee, Int. J. Hydrogen Energy 32 (15) (2007) 3442–3447.
[45] A. Venkatasubramanian, M. Navaei, K.R. Bagnall, K.C. MacCarley, S. Nair, P.J. Hesketh, Gas adsorption characteristics of metal-organic frameworks via quartz crystal microbalance techniques, J. Phys. Chem. C 116 (29) (2012) 15313–15321.
[46] M.F. Cansizoglu, E. Badradee, T. Karabacak, Hydrogen storage properties of magnesium nanotrees investigated by a quartz crystal microbalance system, Int. J. Hydrogen Energy 43 (29) (2018) 21844–21855.
[47] A. Kubota, H. Miyaoka, M. Tsubota, K. Shimoda, T. Ichikawa, Y. Kojima, Synthesis and characterization of magnesium-carbon compounds for hydrogen storage, Carbon 56 (2013) 50–55.
[48] B.D. Cullity, Elements of X-Ray Diffraction, second ed., Addison-Wesley, 1978.
[49] S. Brunauer, P.H. Emmett, E. Teller, Adsorption of gases in multimolecular layers, J. Am. Chem. Soc. 60 (2) (1938) 309–319.
[50] J. Boa, N. Kishi, I. Khatri, T. Soga, T. Jimbo, Catalyst-free synthesis of carbon nanofibers by ultrasonic spray pyrolysis of ethanol, Mater. Lett. 68 (2012) 240–242.
[51] F.-W. Wang, T.-C. Lin, S.-D. Tzeng, C.-T. Chou, Field emission properties of carbon nanotubes cathodes produced using composite plating, Appl. Surf. Sci. 256 (2010) 7600–7605.
[52] W. Cho, M. Schulz, V. Shanov, in: Satoru Suzuki (Ed.), Kinetics of Growing Centimeter Long Carbon Nanotube Arrays, Syntheses and Applications of Carbon Nanotubes and Their Composites, 2013.
[53] R. Zacharia, K.Y. Kim, S.W. Hwang, K.S. Nahm, Intrinsic linear scaling of hydrogen storage capacity of carbon nanotubes with the specific surface area, Catal. Today 120 (2007) 426–431.
[54] S. Bianco, M. Giorcelli, S. Musso, M. Castellino, F. Agresti, A. Khandelwal, S. Lo Ruso, M. Kumar, Y. Ando, A. Tagliaferro, Hydrogen adsorption in several types of carbon nanotubes, J. Nanosci. Nanotechnol. 10 (2010) 3860–3866.
[55] M. Elyassi, A. Rashidi, M.R. Hantehzadeh, S.M. Elahi, Hydrogen storage behaviors by adsorption on multi-walled carbon nanotubes, J. Inorg. Organomet. Polym. Mater. 27 (1) (2017) 285–295.
[56] S.U. Rather, Trimetallic catalyst synthesized multi-walled carbon nanotubes and their application for hydrogen storage, Kor. J. Chem. Eng. 33 (5) (2016) 1551–1556.
[57] G.E. Ioannatos, X.E. Verykios, H2 storage on single- and multi-walled carbon nanotubes, Int. J. Hydrogen Energy 35 (2010) 622–628.
[58] M.S. Dresselhaus, G. Dresselhaus, Intercalation compound of graphite, Adv. Phys. 30 (1981) 139–326.
[59] M.S. Dresselhaus, K.A. Williams, P.C. Eklund, Hydrogen adsorption in carbon materials, MRS Bull. 24 (11) (1999) 45–50.
[60] M.R. Pederson, J.Q. Broughton, Nanocapillarity in fullerene tubules, Phys. Rev. Lett. 69 (1992) 2689–2692.